Recent developments and physics prospects for ICRH on W7-X

<u>J.Ongena</u>[1], Ye.O.Kazakov[1], V.Borsuk[2], F. Durodié[1], D.A.Hartmann[3], K-P. Hollfeld[4], J.P. Kallmeyer[3], F.Louche[1], A.Messiaen[1], D.Nicolai[2], G.Offermanns[4], B.Schweer[1], I.Stepanov[1], M.Vervier[1], D.Birus[3], A.Dinklage[3], J.Faustin[3], A.Krivska[1], O.Neubauer[2], M.Van Schoor[1], R.C.Wolf[3] and the W7-X team[3]

[1]*Laboratory for Plasma Physics, Ecole Royale Militaire-Koninklijke Militaire School, 1000 Brussels, Belgium, TEC Partner*
[2]*Institut für Energie- und Klimaforschung / Plasmaphysik (IEK-4), TEC Partner, Forschungszentrum Jülich, D-52425 Jülich, Germany*
[3]*Max-Planck-Institut für Plasmaphysik, Wendelsteinstraße 1, D-17491 Greifswald, Germany*
[4]*Zentralinstitut für Engineering, Elektronik und Analytik –Engineering und Technologie, (ZEA-1), Forschungszentrum Jülich, D-52425 Jülich, Germany*

1. Introduction

The stellarator Wendelstein 7-X (W7-X) started first plasma operation in December 2015, which lasted until March 2016. A first very successful experimental campaign OP1.1 confirmed the functionality of the main basic systems and diagnostics [1]. The main heating system used in this first campaign was ECRH at 140 GHz up to 4.3MW. For the next experimental campaigns in 2017-2018 (OP1.2a and OP1.2b) the ECRH power will be further increased to 9MW, complemented by H-NBI heating in pulses up to 10 s. In addition, an ICRH system is under construction. In a first phase, this system aims at coupling 0.5-1MW of RF power within the frequency range 25-38 MHz, using a two-strap antenna [2]. The ICRH system is intended to be ready for the operational phase OP1.2b of W7-X.

An important aim of W7-X is to demonstrate improved fast-ion confinement at volume averaged beta values up to 5% [3]. The highest beta values correspond to plasma densities above 10^{20} m^{-3}. Mimicking the behaviour of alpha particles requires the presence of fast ions in the core of W7-X plasmas with energies in the range 50-100 keV. This is a challenging task, given the expected high plasma densities. However, such a population can be created using Ion Cyclotron Resonance Heating (ICRH) using the newly developed [4] and recently experimentally verified three-ion heating scenario [5]. This scenario allows for strong RF power absorption by a tiny amount of resonant ion species (‰ level) heated at the fundamental cyclotron resonance and as a result increase the efficiency of fast-ion generation. We note that ICRH in W7-X can also provide plasma heating and current drive and will also be used for plasma startup and ICRH wall conditioning.

2. Main design challenges for the Wendelstein 7-X ICRH antenna

The ICRH antenna consists of two poloidal straps. Each strap is connected to a tuning capacitor (2-200 pF) on one side and grounded to the antenna box at the other end [2]. To reduce the voltage in the feeding transmission lines and matching system, a pre-matching has been implemented by connecting the RF transmission lines at an intermediate position to each strap (Fig. 1). The strap width, strap length and antenna box depth have been optimized to maximise the power delivered to the plasma, using a reference plasma density profile in front of the antenna, provided by the W7-X team. The ANTITER, CST Microwave Studio (MWS) and TOPICA codes were used for the antenna design optimization. The calculations have been checked experimentally using a smaller size mock-up antenna together with $BaTiO_3$ as simulation for the plasma load [6]. To maximise coupling, the shape of the two-strap ICRH antenna is carefully matched to the 3D shape of the last closed magnetic surface (LCMS) of the standard magnetic field configuration (m/n=5/5) in W7-X. The surface of the antenna thus

shows a curvature in both the toroidal and poloidal direction. Manufacturing an antenna with such a complex 3D shape requires state-of-the-art Computerized Numerical Control (CNC) mechanical construction equipment. A test stand is currently under construction to check the mechanical, thermal, electromagnetic and vacuum properties of the antenna system. To cope with different magnetic configurations and for RF coupling optimization, inward/outward radial positioning of the antenna and a local gas puffing system are included in the design.
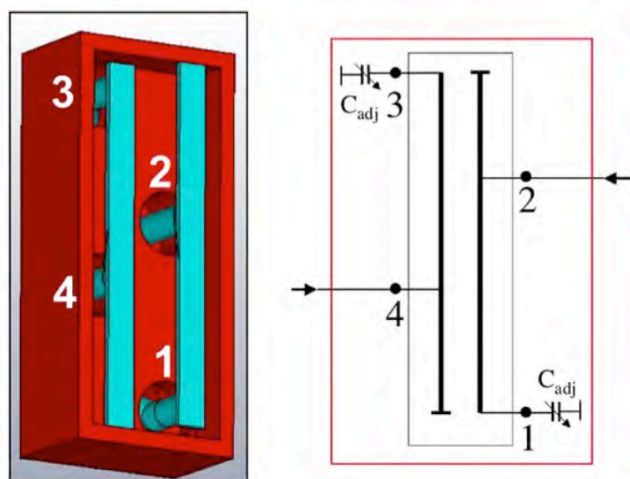

Fig. 1: Schematic view of the W7-X ICRH antenna and its equivalent circuit [5].

3. Mechanical design

An overview of the full system is presented in Fig.2. The antenna head consists of a low cobalt stainless steel box (SS1.4429, Co≤500ppm) with a height of 924 mm and width of 378 mm. The two straps are 866 mm high and 90 mm wide, with a thickness of 15 mm and the distance between the straps is 80mm. To avoid short-circuiting of the straps to antenna box or plasma by the magnetic field lines, the straps are recessed inside the antenna box by 10 mm with an additional option for 15mm. The ICRF power will be delivered by the former TEXTOR RF generators, capable of delivering up to 2MW each in pulses of max. 10s in the frequency range 25-38 MHz. In a first phase only one generator will be connected, allowing monopole $(0, 0)$ and dipole $(0, \pi)$ phasing of the straps. In a second phase, using the two generators simultaneously, the ICRH antenna phasings can be extended to excite the asymmetric spectra $(0, \pm\pi/2)$, $(0, \pm\pi/4)$, etc.

The plasma facing surfaces of the antenna box are shielded with graphite tiles that are also shaped according to the LCMS of the standard magnetic configuration within ±0.3 mm accuracy [7]. The heat load from the plasma is removed by cooling water channels underneath the tiles and near the rear side of the box. When not in use, the antenna is retracted into its port duct (labelled AEE31 on W7-X). During operations the antenna can be moved radially over 350mm (with a speed of 3 mm/s) to come as close as possible near the LCFS of the magnetic configuration in use. This speed is sufficient in order to avoid a too large increase in temperature from plasma irradiation during the retraction of the antenna into the port.

The temperature distribution in the cross-section of the graphite and stainless steel wall parts of the antenna head are modelled with ANSYS, confirmed experimentally with a mock-up irradiated with the electron beam device JUDITH-1 [8]. The test tiles performed splendidly and equilibrium surface temperatures of about 1500 C were obtained with repetitive heat load pulses of 2 MW/m^2 without any damage to the tiles. This is far more than the design value and also what is expected during W7-X plasmas with 10MW additional heating. The surface temperature is mainly influenced by CW irradiation from the W7-X plasma, and is in the worst case (a detached plasma) ~ 100 kW/m^2. During antenna operation the straps receive within the skin depth an additional heat load from the RF current. For the grounding of the antenna box air powered pistons are used to press electrical contacts to the duct. Using this system, the grounding is also guaranteed during movement of the antenna in the port duct.
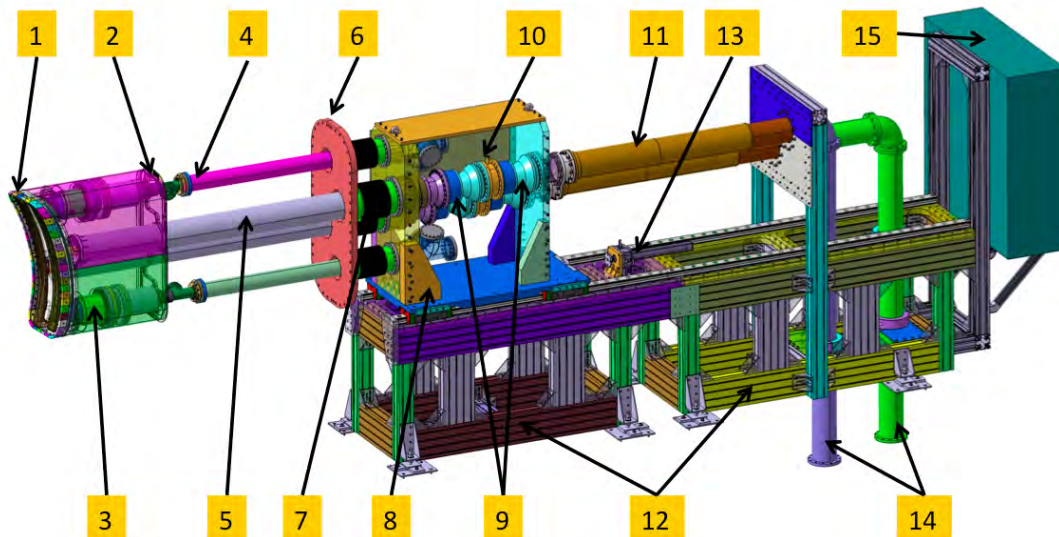
Fig. 2: Overview of the ICRH antenna system under construction for W7-X (1:antenna head with carbon protection tiles, 2:short circuit to AEE31 duct, 3:tunable capacitor, 4:supply tubes for water cooling circuits and diagnostics, 5:coaxial RF transmission line, 6:cryostat flange, 7:bellow, 8:movable antenna support, 9:RF feedthroughs, 10:vacuum control volume, 11:line stretcher, 12:support tables, 13:motor for radial motion of the antenna head assembly, 14:RF lines interface with DC break, 15:electrical cabinet with local control WinCC panel) [7]

The RF power is delivered to the straps through a matching-decoupling system via DC breaks. Two line RF transmission line stretchers (Pos. 11, Fig.2) are included to compensate for the radial movement of the antenna carrier. Each line is foreseen with RF current and voltage probes. The gas puffing system (H_2 or D_2) consists of gas pipes with 1 mm diameter holes at both sides of the antenna head wall and connected with 6 mm diameter gas supply tubes. Two piezo valves mounted at the rear side of the antenna box can deliver 10ms gas pulses. The gas flow can be adjusted by a preset pressure up to 10 bar. Type K thermocouples are foreseen at 8 positions in the graphite tiles along the circumference of the antenna head and at four positions at the capacitor side of the straps. Furthermore, resistive thermal sensors (RTS) Pt100 are mounted at the capacitor housings and at the rear side of the antenna box to monitor the heat load distribution. To measure the electron density profile in front of the ICRH antenna head, a microwave reflectometer consisting of a pair of horn antennas is mounted in the upper and lower part of the rear wall of the antenna head.

3. ICRH scenarios for fast-ion generation and plasma heating on W7-X

For the nominal central toroidal magnetic field $B_0 = 2.5$T, RF power can be deposited to H ($\omega \approx \omega_{ci}$), ^{4}He and D ions ($\omega \approx 2\omega_{ci}$) at the highest RF frequencies available $f \approx 37$–38 MHz. Minority heating of H ions with concentrations of a few % in helium or deuterium plasmas is characterized by strong single-pass wave absorption and has been extensively used in fusion research. This technique can also be applied to generate fast protons at modest plasma densities in W7-X. Fig. 3(a) shows an example of the computed average energy of H ions (X[H] $= n_H/n_e = 3$%) as a function of the central plasma density n_{e0}. Here, we use the SSFPQL code [9] and for simplicity assume the absorbed RF power density by H minority ions $<P_{RF}> = 1$ MW/m^3 as input. In line with the analytical predictions by Stix [10], the tail energies of H minority decrease strongly with increasing n_{e0}. At high plasma densities above 10^{20} m^{-3}, which are of interest for fast-ion confinement studies in W7-X, the efficiency of fast-ion generation with the H minority heating scenario is very limited. We note that the presence of residual H ions sets a constraint on the minimal achievable minority concentration

for this scenario. Furthermore, lowering the hydrogen concentration below 2–3% (if at all possible) would lead to dominant second harmonic absorption by majority ions (helium or deuterium).

The ICRF system of W7-X also allows to heat ^{3}He minority ions ($\omega \approx \omega_{ci}$) at $f \approx 25$ MHz. Efficient generation of energetic ^{3}He ions in dedicated H-D plasmas with $X[H] = n_H/n_e \approx 70$–$80\%$ using the so-called three-ion ICRF scenarios [4,5] was recently demonstrated on JET and Alcator C-Mod. Because intrinsic low-Z impurities such as carbon and oxygen have the same charge-to-mass ratio as D ions ($Z/A = 1/2$), they can replace D in the three ion scenarios. E.g. 3% of carbon impurities have the same effect on wave propagation as 18% of D ions. Thus, the realization of ^{3}He minority heating at extremely low concentrations ($X[^3He] \approx 0.1\%$) in W7-X might simply rely on using H plasmas naturally contaminated with low-Z impurities with $Z/A = 1/2$. We note also the possibility of additional injection of a few per cent of ^{4}He or D ions to fine-tune wave polarization and maximize the efficiency of ^{3}He fast-ion generation. According to 3-D ICRF modeling with the SCENIC code package the number of ^{3}He ions in the energy range above 50 keV is about 20 times larger for the three-ion scenario ($X[^3He] = 0.1\%$) than for the (^{3}He)-H minority heating at $X[^3He] = 2\%$ [11] (see Fig.3(b)).
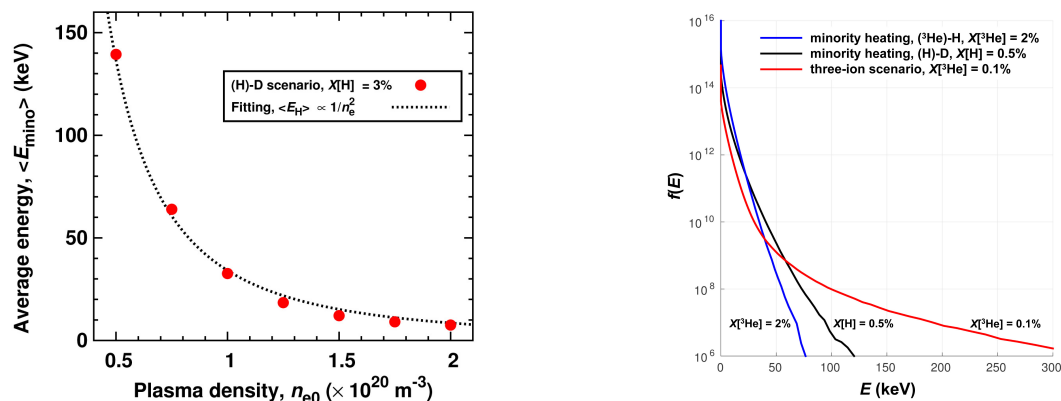

Fig. 3. (a) Average energy of RF-heated heated hydrogen minority ions ($X[H] = n_H/n_e = 3\%$) as a function of the central plasma density computed with the SSFPQL code. We assume $<P_{RF}> = 1$ MW/m^3 for the RF power density absorbed by the H ions. (b) Comparison of the RF-heated energy distribution function for ^{3}He minority ions obtained using the three-ion scenario with $X[^3He] = 0.1\%$ and the ^{3}He minority heating in H scenario where $X[^3He] = 2\%$; we added for comparison also the RF-heated energy distribution function for H minority ions using the (H)-D scenario with $X[H] = 0.5\%$ ($P_{ICRH} = 1.5$ MW, $n_{e0} = 1.5x10^{20}$ m^{-3}, $T_0 = 4$ keV). The figure is reproduced from [11].

4. References

[1] WOLF, R.C. et al., "Major results from the first plasma campaign of the Wendelstein 7-X stellarator", accepted for publication in *Nucl. Fusion* (2017). Available online at: http://dx.doi.org/10.1088/1741-4326/aa770d.
[2] ONGENA, J., MESSIAEN, A.M., et al., *Physics of Plasmas* **21**, 061514 (2014).
[3] BOSCH, H.-S. et al., *Nucl. Fusion* **53**, 126001 (2013).
[4] KAZAKOV, Ye.O. et al., *Nucl. Fusion* **55**, 032001 (2015).
[5] KAZAKOV, Ye.O., et al., *Nature Physics* (2017); http://dx.doi.org/10.1038/nphys4167
[6] ONGENA, J., MESSIAEN, A.M., et al., 25th Fusion Energy Conference (FEC 2014) (13-18 October 2014, Saint Petersburg, Russia), Paper TH/P6-60.
[7] SCHWEER, B., ONGENA, J., BORSUK, V., et al., *Fusion Engineering and Design* (2017), in press; http://dx.doi.org/10.1016/j.fusengdes.2017.05.019
[8] DUWE, R., KÜHNLEIN, W, MÜNSTERMANN, H., Proc. 18th SOFT (Karlsruhe, Germany, 22–26 August 1994), published in Fusion Technology 1994, pp.355–358 (1995).
[9] BRAMBILLA, M. and BILATO, R., *Nucl. Fusion* **49**, 085004 (2009).
[10] STIX, T.H., *Nucl. Fusion* **15**, 737–754 (1975).
[11] FAUSTIN, J.M. et al., *Plasma Phys. Control. Fusion* **59**, 084001 (2017)